PHYSICAL REVIEW B **81**, 245403 (2010)

Site-specific electronic and geometric interface structure of Co-tetraphenyl-porphyrin layers on Ag(111)

Willi Auwärter,[1,2,*] Knud Seufert,[2] Florian Klappenberger,[2] Joachim Reichert,[1] Alexander Weber-Bargioni,[1] Alberto Verdini,[3] Dean Cvetko,[4] Martina Dell'Angela,[3] Luca Floreano,[3] Albano Cossaro,[3] Gregor Bavdek,[4] Alberto Morgante,[3,5] Ari P. Seitsonen,[6,7] and Johannes V. Barth[1,2]

[1]*Department of Physics & Astronomy, University of British Columbia, Vancouver, British Columbia, Canada V6T1Z4*

[2]*Physik Department E20, Technische Universität München, D-85748 Garching, Germany*

[3]*CNR-IOM Laboratorio TASC, Basovizza SS-14, Km 163.5, I-34149 Trieste, Italy*

[4]*Department of Physics, University of Ljubljana, Ljubljana, Slovenia*

[5]*Department of Physics, University of Trieste, Trieste, Italy*

[6]*IMPMC, CNRS and Université Pierre et Marie Curie, 4 place Jussieu, case 115, F-75252 Paris, France*

[7]*Institute of Physical Chemistry, University of Zurich, Winterthurerstr. 190, CH-8057 Zurich, Switzerland*

(Received 12 February 2010; revised manuscript received 28 April 2010; published 1 June 2010)

We present a combined multimethod experimental and theoretical study of the geometric and electronic properties of Co-tetraphenyl-porphyrin (Co-TPP) molecules adsorbed on a Ag(111) surface. Scanning tunneling microscopy (STM) topographs reveal that Co-TPP forms highly regular arrays with a square unit cell. Hereby, the Co-TPP molecules do not occupy a unique adsorption site on the Ag(111) atomic lattice. The central Co atom of the Co-TPP is found to reside predominantly above fcc and hcp hollow sites of the substrate, as determined from the photoelectron diffraction patterns. A strong adsorption-induced deformation of Co-TPP involving a saddle-shaped macrocycle is evidenced by high-resolution STM images and quantified by near-edge x-ray absorption fine-structure measurements. By scanning tunneling spectroscopy we resolved discrete molecular electronic states and mapped the pertaining spatial charge-density distribution. Specifically, we discuss the interaction of orbitals originating from the Co-metal center with the porphyrin macrocycle and show that the varying adsorption sites induce a modulation in the Co-TPP lowest unoccupied molecular orbital. These findings are corroborated by density-functional-theory calculations.

DOI: 10.1103/PhysRevB.81.245403 PACS number(s): 68.43.−h, 73.20.−r, 33.15.Bh, 81.16.Dn

I. INTRODUCTION

The control of large organic molecules and their supramolecular assembly on well-defined substrates currently attracts considerable interest[1,2] as it plays a crucial role in various fields in science and technology, ranging from heterogenous catalysis[3,4] to molecular spintronics,[5] electronics,[6,7] and optoelectronics[8,9] based on organic thin films[10] or single-molecule contacts.[11–13] Especially metalloporphyrins exhibit an intriguing variety of functional properties, which are exploited in both biological and artificial systems.[14,15] Accordingly, these versatile molecules are promising building blocks to assemble functional nanostructures on surfaces, specifically opening up new opportunities to build sensors and nanoscale optical and magnetic materials.[16,17]

Hereby, two interrelated features are the key to the porphyrins' functional properties. First, the central metal ion plays the role of an active site. Besides the coordination to the porphyrin macrocycle, it can interact with a supporting surface and/or bind additional axial ligands.[18,19] Accordingly, the electronic structure of the metal center, which is codetermined by the underlying substrate atoms, dictates the functional properties, steering, for example, the catalytic reactivity or magnetic behavior. This represents a key issue in the emerging field of surface-confined coordination chemistry, aiming at the control of the interplay between lateral metal-ligand interactions and surface bonding.[20,21]

Second, the rotational degrees of freedom of the chosen *meso*-substituents and the flexibility of the porphyrin macrocycle allow for a conformational adaptation of the molecule to its local environment.[22–26] Accordingly, the interaction of metalloporphyrins with a substrate can induce modifications of the molecular configuration,[27–33] such as a distorted macrocycle with a shifted position of the metal center. This, in turn, might evoke a change in chemical reactivity, induced charge transfer or altered magnetic properties.[32] Thus it is of fundamental interest to comprehensively characterize the molecule/substrate interface. This includes a quantitative determination of the internal conformation of the molecule, effects of the registry of the molecule to the substrate atomic lattice, and the electronic level alignment at the interface.

Whereas scanning tunneling microscopy (STM) is well suited to image porphyrins on conducting substrates,[27–30,34–41] and scanning tunneling spectroscopy (STS) can furthermore characterize the electronic structure of the adsorbed porphyrins,[42,43] precise information on the molecular conformation is often elusive to STM measurements as both geometric and electronic contributions influence the STM images. To tackle this issue, we complement the local STM results by photoelectron diffraction (PED) and near-edge x-ray absorption fine-structure (NEXAFS) measurements as well as density-functional-theory (DFT) calculations.

By focusing on Co-tetraphenyl-porphyrin (Co-TPP) on Ag(111), this paper addresses an archetypical metalloporphyrin/metal interface with unprecedented detail. To this end, Sec. III A presents STM results on the self-assembly of Co-TPP/Ag(111). Information on the chemical

state and on the registry of Co-TPP to the Ag(111) surface lattice is given in Sec. III B. Section III C describes the adsorption-induced adaptation of the molecular conformation. Subsequently, the electronic structure of the Co-TPP/Ag(111) interface is discussed in depth in Sec. III D.

II. EXPERIMENTAL SECTION

All STM experiments were performed in a custom-designed ultrahigh-vacuum apparatus comprising a commercial low-temperature STM (Ref. 44) based on a design described in Ref. 45. The system base pressure is below 2×10^{-10} mbar.

The Ag(111) single-crystal surface was cleaned by repeated cycles of Ar^+ sputtering (800 eV) followed by annealing to 730 K. Subsequently, Co-TPP was deposited by organic molecular-beam epitaxy from a quartz crucible held at 625 K. Typical evaporation rates are roughly 0.02 monolayer/min (one monolayer corresponds to a densely packed molecular film). Co-TPP was thoroughly degassed prior to any experiments resulting in a background pressure in the 10^{-10} mbar range during deposition. In our experiments we used both Co-TPP acquired from a commercial supplier (Sigma-Aldrich) and Co-TPP synthesized by the Ruben group at INT Karlsruhe.[46] Only the latter could be applied for high-quality experiments, as the commercial Co-TPP contained up to 50% of H_2-TPP, as determined by x-ray photoelectron spectroscopy (XPS) and confirmed by STM measurements.

After dosing Co-TPP at room temperature, the sample was cooled down and transferred into the STM, where constant current images were recorded at $T \sim 6$ K using electrochemically etched tungsten tips. In the figure captions V_b refers to the bias voltage applied to the sample and I to the tunneling current. Differential conductance data (dI/dV spectra and maps) were obtained by lock-in technique with a typical bias modulation amplitude of 18 mV rms and a frequency of 969 Hz (spectra) and 2.97 kHz (maps). The feedback loop was open for point spectroscopy and closed for dI/dV mapping.

The NEXAFS data were taken at the HE-SGM beamline at BESSY II in Berlin. The carbon K edge was recorded in the partial electron yield mode (retarding voltage 200 V) with a monochromator grid with 1500 lines/mm and slit widths of 200 μm corresponding to an energy resolution of approximately 0.4 eV. All spectra have been referenced against a characteristic peak (285 eV) in simultaneously recorded spectra of a contaminated Au grid. For each incidence angle an average of four spectra is presented. To concentrate on the information related to the Co-TPP adsorbate layer, we processed the raw data by subtracting the signal of the bare crystal, resulting in a pre-edge intensity of 0, then corrected for the nonconstant transmission through the beamline and finally normalized the edge jump to one at an energy of 330 eV.

The PED experiments were performed at the ALOISA beamline[47] of the Elettra Synchrotron Light Source in Trieste, Italy. The PED polar scans have been measured by collecting the photoemission signal as a function of the polar emission angle by rotating the electron analyzer in the scattering plane for different orientations of the surface azimuth. The incidence angle of the photon beam was kept fixed at 4° with the polarization in the transverse magnetic condition and the surface normal in the scattering plane.

The Co $2p_{3/2}$ photoemission core line has been selected for the PED measurements with a kinetic energy of 260 eV (photon energy of 1040 eV), in order to have a good compromise between photon flux, energy resolution, and PED signal-to-noise ratio. The angle-resolved intensity $I(\theta, \phi)$ was measured for polar angles θ up to 68° and for azimuthal angles ϕ over a range of 64°, including the two nonequivalent symmetry directions $[11\bar{2}]$ and $[2\bar{1}\bar{1}]$ of the underlying Ag substrate. The sample was kept at about 170 K during the measurements, in order to minimize radiation damage due to secondary electron emission. No difference in the XPS spectra of Co, C, and N has been detected after 12 h of illumination of 1 keV x-rays.

The deposition of Co-TPP[46] has been monitored by means of a quartz microbalance. In contrast to the sample preparation for the STM measurements, where mainly submonolayer coverages of Co-TPP were applied, the synchrotron experiments are based on coverages of one monolayer or more. To prepare a fully saturated monolayer, a Co-TPP multilayer was deposited and subsequently reduced to a single monolayer by thermal desorption of the multilayer (annealing at 250 °C for 300 s). For the Co-TPP/Ag(111) system, this procedure yields the same monolayer structure as direct deposition.[48]

Reflection high-energy electron diffraction (RHEED) patterns have been collected *in situ* along the $[\bar{1}\bar{1}2]$ and $[\bar{1}10]$ directions of the substrate. Care has been taken to avoid film damaging by RHEED primary and secondary electrons, so RHEED exposures prior to x-ray measurements were always kept as short as possible.

We performed DFT calculations using the local-density approximation (LDA) as the exchange-correlation functional, because there is a fundamental problem regarding the description of the interaction between aromatic molecules and noble-metal surfaces when applying the generalized gradient approximations, which would otherwise be more accurate. Calculations in LDA have yielded good results regarding the adsorption of large π-orbital molecular systems, due to approximate compensation for the lack of van der Waals interactions by the LDA tendency to overestimate binding energies.[49–51]

We used the VASP code (Ref. 52) for the calculations. The Kohn-Sham orbitals were expanded in a plane-wave basis up to a cut-off energy of 37 Ry and the core-valence interaction was treated with the projector-augment wave method.[53,54] The substrate was modeled with three layers of Ag, of which the uppermost was allowed to relax, and we saturated the opposite side with hydrogen at the fcc sites. The difference of the asymptotic potential at the opposite sides of the slab was treated with an electrostatic dipole in the vacuum region of ~10 Å between the molecule and the saturating hydrogen atoms. We relaxed the structure with a (2×2) mesh of Monkhorst-Pack k points and analyzed the electronic structure with a (4×4) mesh. The occupation numbers were

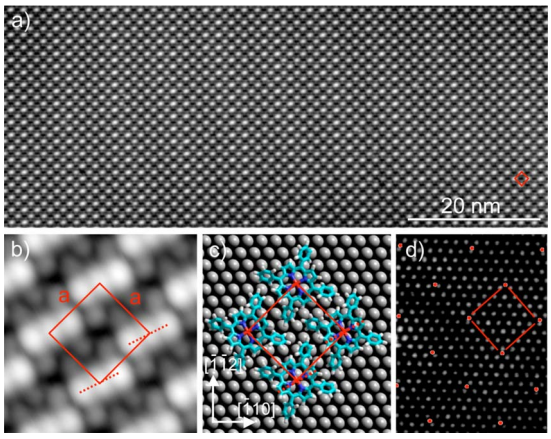

FIG. 1. (Color online) Co-TPP assembly on Ag(111): (a) large-scale topographic STM image. Every protrusion corresponds to a Co-TPP molecule (V_b=−0.48 V and I=97 pA). The red square marks the unit cell. (b) Detailed image showing submolecular resolution. Besides the molecular main axis (three aligned maxima, dashed line) four dimmer protrusions corresponding to the phenyl groups can be identified (V_b=−0.9 V and I=0.12 nA). The molecular packing is described by a square unit cell with side length $a=14.05\pm0.2$ Å. (c) Structural model of the unit cell. (d) Superposition of the Ag(111) atomic lattice (V_b=−13 mV and I =4.9 nA) and the Co positions (red dots) in a Co-TPP array extracted from an STM image. This figure highlights the azimuthal orientation of the Co-TPP domain depicted in (b) relative to the Ag(111) atomic lattice (nearest-neighbor distance a_0=2.89 Å) and indicates the higher-order coincidence structure of the overlayer (see text for discussion).

broadened with the Fermi-Dirac distribution of 50 meV width.

The lateral size of the supercell was chosen to be rectangular with dimensions 20.56×20.35 Å^2, containing 56 substrate atoms per layer; this corresponds to the experimental case of an isolated molecule at the substrate. We studied three atomic geometries where the Co atom at the center of the molecule was placed on-top, hcp and bridging the substrate atoms in the topmost layer; in the latter case we fixed the lateral coordinates of the Co atom, practically freezing the lateral position of the molecule.

III. RESULTS AND DISCUSSION

A. Self-assembled Co-TPP arrays: Ordering and registry to the Ag(111) substrate

Figure 1(a) shows an STM image of a highly ordered Co-TPP array self-assembled after room-temperature deposition. Due to the high mobility of Co-TPP on Ag(111) at room temperature, these islands reach extensions of several hundreds of nanometers, even at coverages well below one monolayer. Figure 1(b) highlights the molecular ordering. We observe a square unit cell (side length $a=14.05\pm0.2$ Å and angle $90°\pm2°$) which agrees with earlier room-temperature results of Co-TPP on Ag(111) (Ref. 55) and Au(111).[40] In contrast to these studies, the submolecular resolution allows us to determine the orientation of the Co-TPP within the layers and to precisely determine the dimensions of the unit cell and its orientation relative to the underlying Ag(111) atomic lattice [cf. Fig. 1(d)]. These STM images exhibit distinct intramolecular features that show a voltage-dependent contrast (see Sec. III D). We use the elongated protrusion dominating the images at negative bias voltages to define the main axis and associate the four smaller lateral protrusions with the *meso*-groups,[33,29] an assignment confirmed by the molecular dimensions (side length ~12 Å). The twofold symmetric appearance signals that the molecules' conformation after adsorption differs from that of the free species (where the macrocycle has a fourfold symmetry) and points to a new conformation characterized by a nonplanar macrocycle deformation. This adsorption-induced distortion of Co-TPP will be discussed in a quantitative manner in Sec. III B and is assigned to a saddle-shaped macrocycle geometry. The imaging characteristics of Co-TPP summarized in Fig. 1 are in line with observations of Co-TPP on Cu(111),[43,56] Au(111),[56] and other metalloporphyrins on Ag(111) (Ref. 33) and complete earlier room-temperature data of Co-TPP on Ag(111).[55]

The main axes of the molecules within one island are all aligned in parallel [Fig. 1(b)] and follow the $\langle11\bar{2}\rangle$ high-symmetry directions of the Ag(111) substrate, as inferred by imaging the atomic lattice. Thus, three possible azimuthal orientations of Co-TPP on Ag(111) exist, which are all observed in the experimental data.

In addition one diagonal of the unit cell is aligned with the Ag(111) $\langle\bar{1}10\rangle$ close-packed directions and the other diagonal with the $\langle\bar{1}\bar{1}2\rangle$ directions. Accordingly, six possible domains of Co-TPP assemblies exist and are observed in the experiments. Hereby, we deal with three domains rotated each by 120° and their respective mirror domains. Figure 1(c) depicts a structural model of the unit cell and its azimuthal orientation relative to the Ag(111) atomic lattice for the domain present in Fig. 1(b). A close inspection of Fig. 1(c) reveals that the phenyl legs of neighboring molecules are oriented in a T-type manner. Such a T-type geometry, where the H atom of one ring points toward the center of the adjacent ring is well characterized by calculations for benzene dimers.[57,58] This arrangement is known to induce attractive interactions and thus stabilizes the molecular assembly.[56] At the same time, this coupling mechanism also explains the occurrence of six domains. With respect to an arbitrary Co-TPP molecule, which follows one of the three possible orientations, an adjacent molecule has two equivalent positions: it can be laterally offset either to the right or to the left of the main axis. In contrast, a related pyridyl-terminated porphyrin species (TPyP) assembles in a more complex arrangement exhibiting two different molecular orientations per unit cell.[29]

It is important to note that the unit-cell dimensions prevent a commensurate order of the Co-TPP layer on the Ag(111) lattice. This is directly visualized in Fig. 1(d), where an STM image taken on a bare Ag(111) patch resolving the atomic lattice is superimposed on a topograph highlighting only the central part of Co-TPP molecules in an island. While the absolute translational position of the two images is arbitrary, the azimuthal orientation and the length scale are

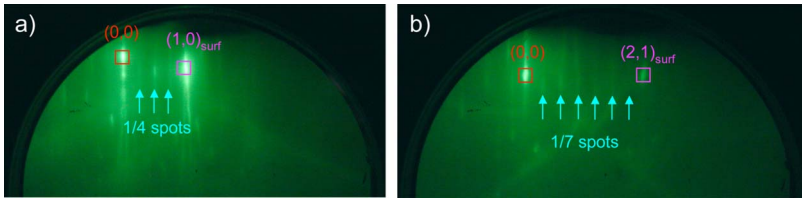

FIG. 2. (Color online) RHEED patterns (15 keV) taken after Co-TPP deposition at room temperature and postannealing to 525 K. (a) The 1/4 spots point to a superstructure with a fourfold substrate periodicity along the $[\bar{1}\bar{1}2]$ direction of the Ag substrate. (0,0) indicates the spot of the reflected specular beam. (b) The 1/7 spots of the superstructure along the $[\bar{1}10]$ direction.

identical. It indicates that the Co-TPP molecules occupy varying positions on the Ag lattice, in agreement with the unit-cell parameters determined from many images. Nevertheless, the unit-cell parameters do not deviate strongly from a coincidence fit: the molecules on the diagonals of the unit cell are separated by 19.9 Å and occupy nearly identical sites, which are, however, different for the two diagonals [see Fig. 1(c)]. The impact of this noncommensurate adsorbate structure on the electronic structure at the interface will be addressed in Sec. III D in some more detail. It should be noted that noncommensurate overlayers are often characterized by long-range height modulations apparent in topographic STM images, so-called Moiré patterns.[29,59] This effect is also observed for the present system, however, it is very subtle (cf. Sec. III D).

The ordering and the azimuthal orientation of the Co-TPP arrays relative to the Ag(111) substrate determined on a local scale by STM are confirmed by space-averaged reflection RHEED experiments. The RHEED patterns reported in Fig. 2 clearly show three intensity maxima along the $[\bar{1}\bar{1}2]$ direction between principal spots of the Ag substrate, indicating a superstructure with fourfold periodicity and a somewhat distorted sevenfold periodicity along $[\bar{1}10]$. These superstructure spots can be related to the square unit cell observed by STM, whose diagonals are oriented along $\langle\bar{1}\bar{1}2\rangle$ and $\langle\bar{1}10\rangle$ directions. Assuming a precise sevenfold periodicity along the $[\bar{1}10]$ direction we obtain an intermolecular distance of $7a_0$=20.23 Å, where a_0=2.89 Å is the nearest-neighbor distance for Ag atoms. A perfect fourfold periodicity along $[\bar{1}\bar{1}2]$ yields $4\sqrt{3}a_0$=20.01 Å. These values are very close to the experimentally determined length of the diagonals of 19.9 Å. However, these observations do not reveal anything about the absolute positions of the Co-TPP molecules with respect to the Ag atomic lattice. Therefore, in addition to the information on the ordering discussed so far, we performed a detailed PED study to get further insights into possible adsorption sites of Co-TPP within the highly ordered molecular arrays on Ag(111).

B. Photoelectron diffraction on Co-TPP/Ag(111)

In order to obtain the PED patterns, XPS of the Co $2p_{3/2}$ peak have been collected at different emission angels, sampling the angular distribution of the outgoing photoelectrons in the azimuthal range including the two nonequivalent $[\bar{2}11]$ and $[\bar{1}\bar{1}2]$ symmetry directions and a polar-angle range extending from 0° to 68° with respect to the surface normal. A typical XPS spectrum taken with a photon energy of 1040 eV is shown in Fig. 3(a). It was recorded on about three monolayers of Co-TPP/Ag(111) to identify components stemming from the first layer contacting the substrate and the adjacent, rather decoupled layers. Clearly, the spectrum shows differ-

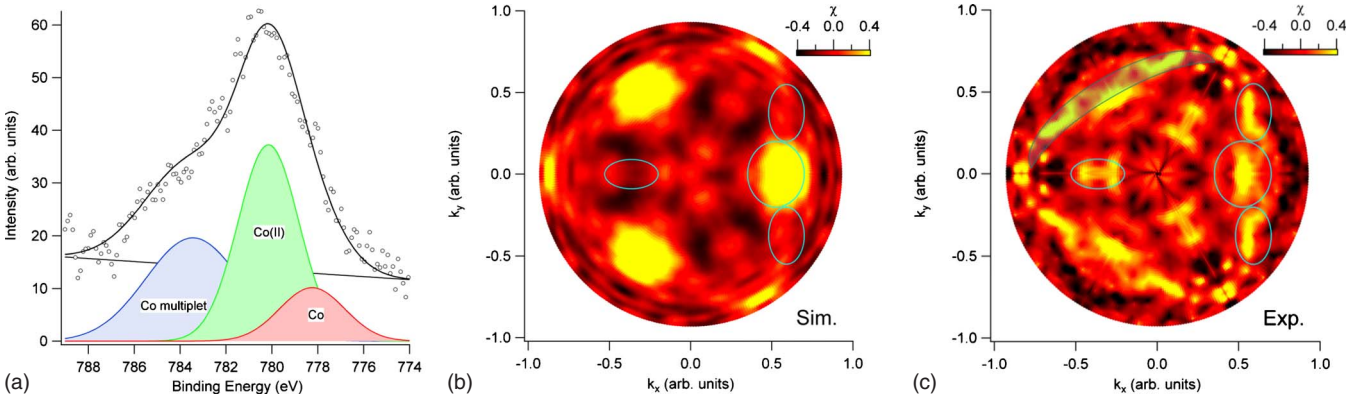

FIG. 3. (Color online) (a) Co $2p_{3/2}$ x-ray photoelectron spectrum on Co-TPP/Ag(111) taken at a coverage of roughly three monolayers (dots) together with the best fit based on three Gaussian functions and a linear background (see text for details). (b) Plot of the 2D PED pattern of the measured anisotropy of the Co $2p_{3/2}$ emission (kinetic energy of 262 eV) from the Co(0) peak. The experimental polar range extends from 0° to 68° with respect to the surface normal. The blue lines highlight the main features. The Kikuchi lines are marked by the blue band. (c) Simulated anisotropy χ for Co atoms in both fcc and hcp stacking sites and in substitutional sites in the first two layers of the underlying Ag representing the best fit (see text for discussion).

ent components and cannot be described by a single peak. Following earlier assignments, we discriminate three spectral features and consider these peaks as follows: the peak at 778.2 eV binding energy can be ascribed to Co-TPP molecules of the first monolayer or/and with metallic Co atoms at equal energy [Co(0), labeled Co], the main peak at 780.5 eV originates from the Co-TPP molecules in second and third layers [labeled Co(II)], and the broad peak at 783.8 eV arises from the multiplet structure observed in Co compounds.[40,48] Accordingly the binding-energy difference between Co(0) and Co(II) peaks equals 1.82 eV, in excellent agreement with the value of 1.80 eV reported in Ref. 48, possibly reflecting the substrate core-hole screening effects which lower the measured binding energies. To extract the PED pattern corresponding to the Co(0) emission from the Co center in the Co-TPP monolayer, the spectra were fitted with peak positions and widths fixed and equal to the average values, obtained over extended polar and azimuthal angles, and only the peak intensity was varied.

We first discuss the effect of excess Co-TPP coverage on the single-layer PED pattern. In principle we might expect the monolayer PED pattern to be distorted due to scattering of the outgoing photoelectrons in the following layers. Yet a poorly ordered overlayer hardly superimposes additional diffraction features, but rather smears out the monolayer diffraction signal. A fully ordered crystalline overlayer with square symmetry, on the other hand, would impose a PED pattern with lower orientational symmetry (sixfold or 12-fold), simply because of focusing the PED intensity in the directions of nearby cobalt centers. As such a symmetry lowering has not been observed, we assume that excess coverage Co-TPP molecules do not significantly alter the monolayer PED pattern.

The experimental PED pattern containing the modulations anisotropy, due to the electron diffraction, has been obtained as $\chi(\theta,\phi)=I(\theta,\phi)/I_0(\phi)-1$, where θ is the polar angle measured from the surface normal, ϕ is the azimuthal angle, and $I_0(\phi)$ is the nondiffractive part of the polar scan signal obtained as an average of the polynomial fit of polar scans for each angle ϕ.

The resulting PED pattern corresponding to the Co signal from the first monolayer is reported in Fig. 3(b). The main features are the clearly manifested threefold symmetry and the absence of isotropic bands in the azimuthal direction, indicating that the Co centers occupy highly symmetric sites. Moreover, the presence of so-called Kikuchi lines is a signature of photoelectron emission from inside the crystal and thus indicates that probably some Co atoms reside inside the crystal in a metallic state. The presence of metallic Co atoms might be due to Co-releasing impurities in the molecular powder and/or to Co atoms detached from the porphyrin macrocycle during the postgrowth annealing. As such induced defects were never observed in the STM experiments, the amount of subsurface Co is expected to be rather low.

In order to find the relative position of the Co atoms with respect to the underlying Ag lattice, we compared the experimental PED patterns with the simulated ones. The simulated χ values have been obtained using the MSCD package.[60] The structural models used for the simulation include about 60 atoms, where one Co atom is placed in a high-symmetry site

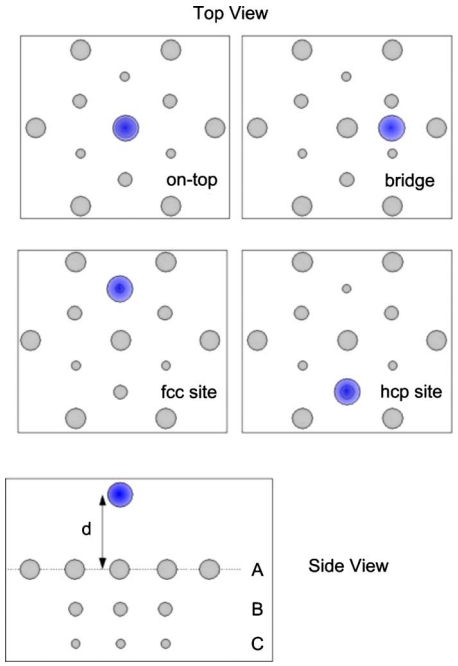

FIG. 4. (Color online) Top and side views of the interface structures of the emitting Co atom (blue circle) placed a distance d above a three layer Ag(111) slab (gray balls) for each model considered in the simulated PED anisotropies.

of a Ag(111) cluster: on-top, bridge, fcc, and hcp stacking positions were considered (see Fig. 4). The distance d between the Co atom and the Ag surface layer has been varied between 2 and 3 Å, which enables a direct comparison with theory. The N atoms of the porphyrin macrocycle were not included in the structural models. This simplification is justified, since the polar range ($\theta_{max}=68°$) does not cover the angles where any forward focusing effects along the Co-N bond direction are expected. Moreover, multiple scattering effects due to the N atoms are clearly weaker as compared to Ag, due to the big difference in the atomic number and thus in the scattering cross-section ($Z_N=7$ vs $Z_{Ag}=47$). In order to discriminate between possible arrangements of Co-TPP on Ag(111), we compared the anisotropy functions χ_{sim} calculated for different adsorption sites, including multiple sites, with the experimental data (χ_{exp}). This comparison is based on the following reliability factor R:

$$R_f=\frac{\sum(\chi_{exp}-\chi_{sim})^2}{\sum(\chi_{exp}^2+\chi_{esim}^2)}.$$

Multiple configurations for the Co atom residing at a distance d over the on-top and bridge sites of the (111) Ag lattice did not yield any satisfactory agreement with the experimental PED pattern. In fact, the obtained reliability R factors were consistently found above the value of $R=1$.[61] Also the overall visual resemblance of the performed simulations with the experimental data was rather poor which permitted us to exclude both structural models from further considerations.

The two hollow adsorption sites (i.e., fcc and hcp types) on the other hand proved to be a much better choice for the simulation model. For pure hcp and fcc model sites considerably lower R factors (minimum value $R_{\mathrm{fcc}}=0.7$ and $R_{\mathrm{hcp}}=0.9$) were obtained for best-fit values of $d_{\mathrm{fcc}}=2.4\pm0.1$ Å and $d_{\mathrm{hcp}}=2.5\pm0.1$ Å. We further note that the same Co-TPP overlayer may geometrically provide both "hollow" adsorption sites for the central Co atoms. We indeed find further improvement of the simulated PED pattern with the experiment by including both fcc and hcp sites in equal shares ($R_{\mathrm{fcc+hcp}}=0.67$). Further reduction in the R factor could be probably achieved by fine tuning of several site related parameters (e.g., relative share of the fcc/hcp sites, spatial displacements from the high-symmetry site, vertical displacement d), yet such calculation intensive analysis is beyond the reach of the present work. We hence conclude that Co atoms predominantly reside at or close to threefold hollow sites, 2.5 ± 0.1 Å above the topmost Ag layer, whereas adsorption in the on-top and bridge sites may be excluded.

We furthermore checked also if part of the measured PED pattern may originate from the Co atoms diffusing into the substrate. Such Co PED pattern has been modeled by placing substitutional Co atoms in the Ag sites of the two outermost layers. The resulting χ pattern has been combined with the one of the Co-TPP overlayers (with relative intensity 1:5) to yield the best fit with $R=0.58$. The corresponding PED pattern giving best overall agreement is presented together with the experimental data in Fig. 3. As we are not simulating absolute intensities but χ modulations and since the electron scattering of the Co emitter inside the crystal is much different from the scattering in the overlayer, it is not possible to estimate the true amount of Co atoms diluted in the bulk from the relative weights in the modulation function χ.

As described above, the STM measurements and the RHEED patterns evidence the formation of a Co-TPP layer phase with an almost square unit cell on the Ag surface. Here it should be emphasized that one possible way to construct such a unit cell by placing two Co centers along one diagonal of the square on the on-top sites of the substrate and accordingly the other two on the bridge sites, can be discarded after this PED analysis, as it shows no considerable contribution from the Co placed on-top and bridge sites. However, a unit cell exhibiting perfect fcc positions on one diagonal of the square and precise hcp positions on the other one is not consistent with the angles and dimensions determined by our STM data. We therefore conclude that real Co positions might deviate from the exact hollow sites and rather display a quasi-fcc or/and quasi-hcp registry with the underlying Ag(111) lattice. There is full agreement between STM, RHEED and PED experiments that the structures cannot be explained by a unique adsorption site of Co-TPP on Ag(111), a finding that has implications for the spatial modulation within the Co-TPP layers observed by STS (vide infra).

C. Molecular conformation

After discussing the packing scheme of Co-TPP on Ag(111), we now proceed to quantify the adsorption-induced deformation of the molecules. As mentioned in Sec. III A,

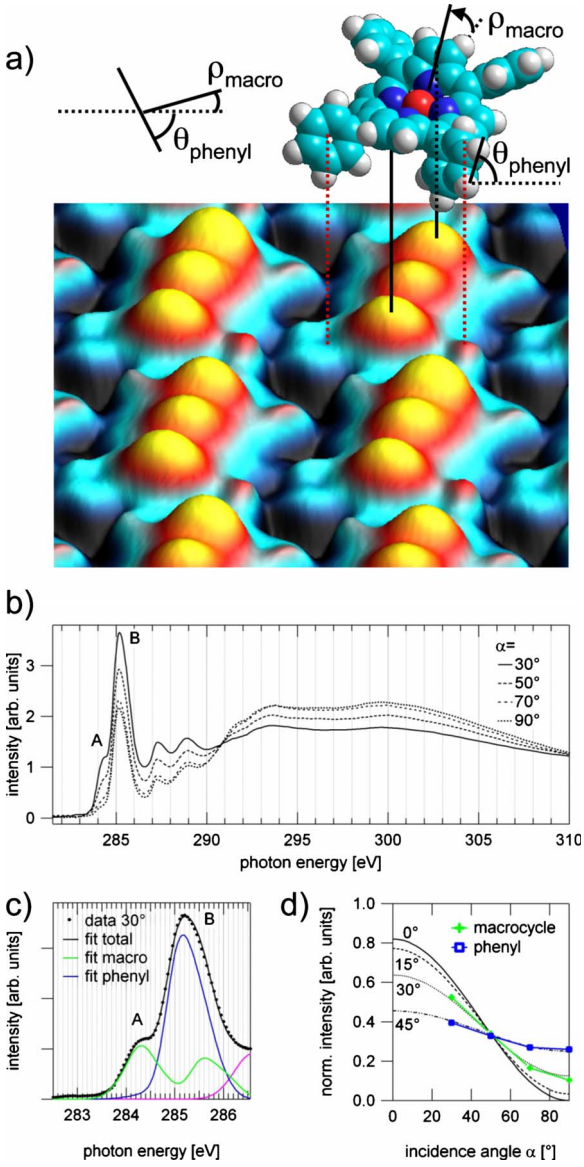

FIG. 5. (Color online) Adsorption-induced deformation of Co-TPP. (a) Pseudo-three-dimensional rendering of a high-resolution STM image suggesting a saddle-shaped macrocycle distortion and alternately rotated phenyl groups ($V_b=-0.7$ V and $I=0.46$ nA). The model represents the geometry consistent with the NEXAFS data displayed in (b). The scheme introduces the angles ρ_{macro} and θ_{phenyl}. (b) Carbon K edge NEXAFS spectra of one monolayer Co-TPP on Ag(111) exhibiting strong dichroism. The different angle dependences of peaks A and B evidence molecular moieties with different orientation with respect to the substrate. (c) Deconvolution of the leading edge into spectral parts originating from the macrocycle (green) and the phenyl groups (blue). (d) The angular dependence of the two moieties yields a nonplanar macrocycle ($\rho_{\mathrm{macro}}=30°$) and rotated phenyl groups ($\theta_{\mathrm{phenyl}}=45°$).

the twofold symmetric appearance of Co-TPP [cf. Fig. 1(b)] points to a conformational adaptation on adsorption. High-resolution images achieved by scanning the Co-TPP using an STM tip modified by a residual gas molecule [cf. Fig. 5(a)] allow us to resolve even more details. Besides the three maxima along the molecular main axis, structures originating

from the phenyl groups are resolved. Following the study of Fe-TPP molecules on Ag(111),[33] the two outer maxima along the main axis are tentatively assigned to two opposite upward bent pyrrole rings expressing the saddle-shaped macrocycle distortion described by an angle ρ_{macro}, whereas the central protrusion originates from the Co. In addition, the outline of the molecule indicates that the phenyl legs are not oriented perpendicular to the molecular core, but alternately rotated by a given angle θ_{phenyl} around the C-C bond connecting them to the macrocycle, as it was observed for a different tetraarylporphyrin species on Ag(111).[29] As pure STM imaging without any additional calculations is generally insufficient to determine the molecular conformation due to contribution from both electronic and geometric effects, we quantify the adsorption-induced distortion of Co-TPP/Ag(111) by angle-dependent NEXAFS spectroscopy, a technique sensitive to the orientation of molecular orbitals with respect to the substrate.[62] This combined STM-NEXAFS approach was successfully applied to resolve the adsorption structure of Co-TPP (Ref. 43) and H_2-TPyP (Refs. 63 and 64) on Cu(111).

The carbon *K* edge spectra of a submonolayer of Co-TPP on Ag(111) are dominated by four peaks in the π^* region (peak A, 284.3 eV; peak B, 285.2 eV; 287.3 eV; and 288.8 eV) and a broad σ^* structure [Fig. 5(b)]. The spectra exhibit a pronounced linear dichroism in dependence of the incidence angle α with α being defined between the electric field vector of the linearly polarized x-ray beam and the surface normal. The comparison to the data set from the Co-TPP multilayer (not shown) highlights that here the peaks are broadened by the interaction with the substrate. Furthermore, the linear dichroism of peaks A and B changes remarkably from the multilayer sample to the monolayer sample. Thus, a pronounced conformational adaptation is imposed on the molecules by the adsorption on the Ag surface. For the quantification of the conformation we proceed to decompose the spectra in parts stemming from the different molecular groups. To this end we focus on the leading edge of the π^* range, where the separation of the spectral features is most reliable. Based on earlier reports we mimicked the typical C 1*s* NEXAFS spectral shape of the phenyl groups[65,66] [Fig. 5(c), blue curve] and that of the macrocycle[67] [Fig. 5(c), green curve] and then fitted the experimental spectrum [Fig. 5(c) solid curve] with a combination of these two components plus an additional peak at higher energies to fit the higher level excitations. For the four spectra with different incidence angle the spectral shape of the two components was kept constant, thus only the three fitting parameters were used to fit the whole series of spectra. Here we have assumed that all Co-TPP molecules adopt uniform adsorption geometries as corroborated by our STM topographs.

The angular dependence of the intensities of the two moieties is given in Fig. 5(d) and is best described by theoretical curves for orientation angles $\gamma_{\mathrm{phenyl}}=45°$ for the phenyl groups and $\gamma_{\mathrm{macro}}=30°$ for the macrocycle, where the orientation angle γ is defined between the surface normal and the dipole moment of the corresponding π^* resonance.

These findings indicate a marked distortion of Co-TPP upon adsorption, in line with the STM results [cf. Figs. 1(b) and 5(a)]. Combining the angles determined by NEXAFS with the symmetries observed in the high-resolution STM images yields the following conformation for Co-TPP on Ag(111). The macrocycle adopts a saddle-shape deformation where one pair of opposite pyrrole rings is tilted upwards by an angle ρ_{macro} of 30° while the other pair bends down by 30°. Moreover, the phenyl legs are rotated by the dihedral angle θ_{phenyl} of approximately 45° out of the surface plane. This value is in perfect agreement with the dihedral angle of 45° suggested for Au-TPP on Au(111).[68]

It should be noted that the dihedral angles of the phenyl groups are related to the macrocycle distortions, as these moieties are coupled by steric interactions. Our results are consistent with recent theoretical predictions correlating the rotation of the phenyl groups with the macrocycle distortion of a free-base TPP.[69] A structural model of Co-TPP in this adsorption geometry is included in Fig. 5(a).

Confirming with this experiment the surface-induced conformational adaptation of the molecules, we address their electronic properties in the following section.

D. Electronic structure at the Co-TPP/Ag(111) interface

A comparison of the STM topographs reproduced in Fig. 6(b) reveals a strong bias dependence of intramolecular features. There are marked differences between images reflecting occupied and unoccupied electronic states obtained at negative and positive bias voltages, respectively. For instance, an elongated protrusion, resulting from the three maxima discussed in the last section, dominates the images at negative voltages [$V_b=-575$ mV, Fig. 6(b) left panel]. Upon tunneling into the unoccupied states [$V_b=925$ mV, cf. Fig. 6(b) second panel from the left], we resolve bright lobes localized over the four mesabridge carbons. Increasing the bias voltage the four protrusions are observed on locations shifted outwards toward the phenyl legs [$V_b=2.38$ V, Fig. 6(b) right panel].

This changing appearance indicates contributions of different electronic channels to the tunneling current arising from the local density of states (LDOS) associated with given molecular orbitals (MOs).[29] We thus explored the pertaining electronic properties by STS. Figure 6(a) compares a spectrum taken on the bare Ag(111) surface, which is dominated by the steplike increase just below the Fermi level (E_{F}) ($V_b=-67$ mV) representing the onset of the surface state with a spectrum on a Co-TPP molecule. The spectrum taken on the Co-TPP molecule shows distinct features absent for the reference spectra on the bare metal. There are four energy regions of interest, which we discuss in detail. Starting at high positive voltages, around 2.3 V, we detect a shoulder in the spectrum (turquoise bar). Around 1 V a broad peak dominates the spectrum (blue bar). At negative bias voltages, we observe a prominent peak at −600 mV (red bar). Finally, around −1.8 V, a faint feature (inset) can be visualized by directly comparing a spectrum taken on the macrocycle with a spectrum taken in the center of the molecule. Before discussing the nature of these electronic states resolved in the spectrum, we explore their spatial distribution by mapping the corresponding charge density. Figure 6(c) shows dI/dV maps taken together with the STM topographs shown in Fig.

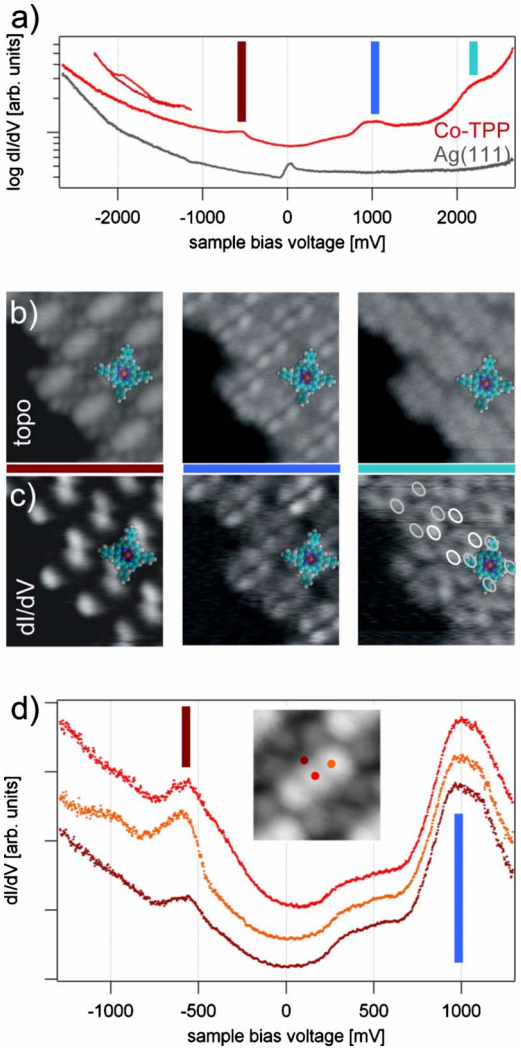

FIG. 6. (Color online) Molecular electronic states of Co-TPP/Ag(111). (a) Tunneling spectra of the bare Ag(111) surface (gray) and over a Co-TPP molecule (red). While the spectrum on Ag(111) only shows the steplike increase around −67 meV related to the onset of the surface state band, three spectral features marked by the colored bars can be easily recognized on Co-TPP (HOMO: −0.6 V, red; LUMO: ~1 V, blue; and LUMO+1: ~2.2 V, turquoise). A faint signal around −1.8 V (HOMO−1) can only be detected by directly comparing a spectra taken on the macrocycle and in the center of Co-TPP (inset). (b) Contrast change in STM topographs for tunneling at specific sample bias voltages as indicated by the colored bars. (c) Visualization of the spectral density of molecular orbitals by dI/dV mapping. The colored bars indicate to which spectral feature in (a) the dI/dV maps correspond. The ovals in the right panel mark the positions of the phenyl groups. (d) Tunneling spectra at three positions on a molecule as indicated in the inset (offset for clarity). These spectra confirm the laterally varying density of states presented in (c) (stabilized at V_b=1 V and I =0.25 nA, see text for further discussion).

6(b). The respective bias voltages were chosen in a way to represent the three peak positions identified above. It is obvious that the state at −575 mV exhibits a twofold symmetry and features a protrusion at each pyrrole group on the main axis, resulting in a characteristic two-lobe structure in the dI/dV map [left panel Fig. 6(c)]. This charge density extends beyond the geometrical structure of the superimposed molecular model. Also for the unoccupied states [the two right panels in Fig. 6(c)], the twofold symmetry is preserved. The latter is, however, less pronounced, because the maps are dominated by four protrusions that are separated by dark lines crossing the center of the molecule. For the state around 2.3 V the weight is shifted to the location of the phenyl substituents. It should be noted that the twofold symmetry of the state at −575 mV is also observed in spectra recorded after stabilizing the tip at a bias voltage, where the molecular core shows a fourfold symmetry [Fig. 6(d)]. Accordingly, a pure topographical origin of the two-lobe structure in the dI/dV maps can be excluded.[70]

The above observations can be rationalized by contrasting them with results from a closely related system, Co-TPP on Cu(111). By comparing dI/dV charge-density maps to extended Hueckel calculations for an isolated Co-TPP molecule, we assigned in a previous study spectral features to specific molecular orbitals of the Co-TPP.[43] Following this procedure, we assign the broad structure around 1 V to the degenerate lowest unoccupied molecular orbital (LUMO) orbitals of Co-TPP. The state at −575 mV is the highest occupied molecular orbital (HOMO), which contains some contribution from the Co d states (vide infra). The feature at −1.8 V is labeled HOMO−1.

The data also reveal that the molecular HOMO carries different weight on upward and downward bent pyrrole groups, respectively. This explains the macrocycle's electronic asymmetry reflected in the twofold symmetric topography and substantiates the NEXAFS interpretation of a conformational adaptation.

Accordingly, analogous to the Co-TPP/Cu(111) case,[43] we can resolve and spatially map specific molecular states. In the following, we focus on the key features of the electronic structure of Co-TPP on Ag(111) and relate them to prior studies on similar systems. To this end, Fig. 7 compares two electronic states for a mixed Co-TPP/H_2-TPP matrix. The topographic image [Fig. 7(b)] clarifies the local structure of the matrix: in the top two rows, each central Co-TPP molecule has two H_2-TPP neighbors. The dI/dV map [Fig. 7(a)] taken at the HOMO energy (−550 meV) shows only the characteristic two-lobe contrast for the Co-TPP, the H_2-TPP molecules are invisible at this energy.[71] This clearly indicates that the HOMO of Co-TPP is related to Co d states and not to a pure porphyrin macrocycle state, as it is absent for the H_2-TPP. This finding is supported by recent STS studies comparing metalloporphyrin species with H_2-TPP (Refs. 55 and 71) and by photoemission experiments on Co-TPP and H_2-TPP/Ag(111).[48] The question is whether we can clarify the character of the involved Co states. Up to now, this state was detected for several Co-porphyrin species in contact with a metal surface and related to the Co d_z^2 orbital.[32,42,48] Whereas an early interpretation, assuming a planar porphyrin macrocycle, assigned the signal to enhanced tunneling mediated by the pure Co d_z^2 orbital,[42] a recent study relates it to a new valence state evoked by an interaction of the Co d_z^2 orbital with Ag sp states.[48] Both views are in line with the results presented in Ref. 32, which shows for Co-TBrPP molecules on Cu(111) that the Co-related HOMO is only de-

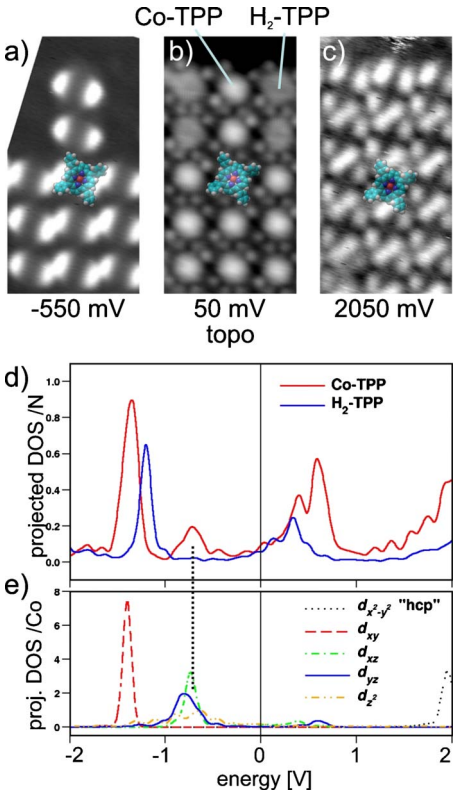

FIG. 7. (Color online) Metal contribution to specific molecular electronic states. (a) dI/dV map representing the density of states corresponding to the HOMO of Co-TPP taken on a mixed Co-TPP/H_2-TPP array represented in the topographic STM image in (b). The spectral electron density originates from Co states, as the corresponding signature is absent for the free base species. Nevertheless, the apparent intensity is peaked on two opposite pyrrole rings (see overlaid model). By contrast, the LUMO+1 orbital represented by the dI/dV map in (c) localized on the phenyl groups is not affected by the metal center [(a)–(c): I=0.6 nA]. (d) Calculated density of states projected on the nitrogen p_z orbitals in H_2-TPP and Co-TPP; only the latter shows the metal-related feature at ~0.7 eV below the Fermi level. (e) Density of states projected on different d orbitals of the central Co atom. At the same energy where the peak on the macrocycle is observed [compare (d) and (a)], d_{xz} and d_{yz} states dominate. The lateral position of the molecules is close to hcp sites.

tected for molecules in a planar conformation, while the very same molecules exhibiting a saddle-shape macrocycle deformation, and accordingly a presumably larger Co-surface separation, exhibit no signal in the corresponding energy window. However, our spatially resolved two-lobe structure clearly indicates that the involved orbital cannot be of pure Co d_z^2 character, as the charge density related to the HOMO orbital is not localized on the Co center, but on two opposite pyrrole rings [cf. Fig. 7(a)]. This points to considerable interactions of the Co d levels with the π system of the porphyrin macrocycle presumably mediated by Co states of d_{xz} and d_{yz} symmetries. The twofold symmetry then reflects the underlying geometric saddle-shape distortion. The finding of a considerable coupling of electronic metal states with orbitals of the porphyrin ligand close to the Fermi level is of importance, as it drastically affects the electronic and magnetic properties of the molecule/substrate system.[5,32]

Our experimental observations are corroborated by DFT calculations of Co-TPP/Ag(111) and H_2-TPP/Ag(111) supercells. Here we focus on two findings most relevant in view of our discussion (the complete account of our extensive DFT modeling will be published elsewhere). In Fig. 7(d) we compare the calculated projected densities of states (PDOS) on the N atoms in the macrocycle of Co-TPP/Ag(111) with H_2-TPP/Ag(111). Importantly, the first pronounced feature in the occupied region only exists for Co-TPP and not for the free-base counterpart, whence it must be related to states of the Co center. This finding, together with the energy position of this spectral feature, allows us to assign it to the HOMO observed in the ST spectra and dI/dV maps of Co-TPP. The key point is that the Co-related density of states is indeed observed on the nitrogen positions of the macrocycle, a finding corroborating the suggested interaction of Co d states with the electronic system of the porphyrin macrocycle. Completive, the PDOS projected on the different orbitals of the central Co atom [cf. Fig. 7(e)] shows strong contribution of Co d_{xz} and d_{yz} states in the relevant energy interval. Another aspect of Fig. 7(d) provides a strong indication that our calculations describe the system well. The experimental finding that the spectral weight related to the LUMO orbital is upshifted when going from H_2-TPP to Co-TPP or other metalated species[33,55,71,72] is successfully reproduced in the PDOS displayed in Fig. 7(d).

Up to now we have shown that the HOMO observed for Co-TPP/Ag(111) is a state originating from Co d_{xz} and d_{yz} orbitals interacting with the π system of the porphyrin, based on C and N atoms of the macrocycle. On the contrary, the LUMO orbital is mainly a porphyrin macrocycle state with minor contribution from the Co center. However, this contribution induces an energy shift of the LUMO of metalloporphyrins compared to the free base species while the symmetry of the LUMO is preserved.[33,55,71] As shown in Fig. 7(c), the LUMO+1 orbital around 2.3 V is not affected by the metal center. The state is localized on the phenyl legs and thus indistinguishable for Co-TPP and H_2-TPP. An inspection of Fig. 7(b) reveals that at very low-bias voltages a central protrusion dominates the STM images in agreement with recent room-temperature observations.[73] This points to a prominent contribution of Co states near the Fermi level (E_F) to the tunneling current. As the protrusion is right at the Co center, the Co d_z^2 orbital might play a decisive role for the observed contrast. Indeed, our DFT calculations [cf. Fig. 7(e)] reveal that the PDOS related to the d_z^2 states is smeared out over a large energy range and reaches to E_F. This broadening might explain why no obvious feature in the dI/dV spectra can be assigned to the d_z^2 orbital. As a matter of fact, spectra taken above the Co center [compare Fig. 6(d)] show a higher intensity in the energy range between the HOMO and E_F than their counterparts measured at off-center positions.

So far we discussed the character, i.e., the origin and the spatial variation in the charge density related to specific molecular orbitals of Co-TPP/Ag(111). Now we want to briefly address another important issue, which is the energy-level alignment of these molecular orbitals relative to the Fermi level of the metal support. In general (cf. Refs. 10 and 74),

the energy of a molecular level with respect to the Fermi level E_F (E_{MO}) is determined by the metal work function ϕ [i.e., the energy difference between E_F and the vacuum level (VL) of the bare metal], the interface shift $\Delta\phi$ of the VL and the binding energy of the molecular level relative to the VL [i.e., the ionization potential (IP) for occupied levels or the electron affinity (EA) for the unoccupied levels]: $E_{MO}=\phi+\Delta\phi+(\text{EA or } -\text{IP})$. The comparison of the energy-level alignment for a given molecular species on different metal substrates points to the interaction strength of the molecule with the substrate. A strong interaction might pin the molecular levels to E_F, thus resulting in identical binding energies E_{MO} for different substrates, but differing values for EA and IP. Very weak interactions would be expressed by an alignment relative to VL, thus resulting in similar values of EA and IP for different substrates while E_{MO} might vary strongly.

For our case, i.e., Co-TPP/Ag(111), all the relevant parameters are known. We identified the binding energies of the molecular levels relative to the Fermi level in our STS spectra (HOMO−1: −1.8 eV, HOMO: −0.6 eV, LUMO: 1 eV, and LUMO+1: 2.3 eV), the work function of bare Ag(111) $\phi\approx4.6$ eV and $\Delta\phi\approx-0.7$ eV are known from literature.[48] Accordingly, we can calculate the binding energies relative to the VL (HOMO−1: −5.7 eV, HOMO: −4.5 eV, LUMO: −2.9 eV, and LUMO+1: −1.6 eV, compare Fig. 8). It is instructive to compare these values with results from Co-TPP and Ni-TPP on Au(111). Scudiero *et al.*[42] observed electronic Co-TPP states at binding energies of −1.2 eV, −0.1 eV, and 1.7 eV relative to the Fermi level of Au(111). We now translate these values to binding energies relative to the VL. Hereby we use the known work function of Au(111) $\phi\approx5.2$ eV and a $\Delta\phi$ of −0.7 eV. This value $\Delta\phi$ for one monolayer Co-TPP on Au(111) is not determined experimentally, but as the cases of Co-TPP/Ag(111) (Ref. 48) and Co-TPP/Cu(111) (Ref. 75) yield the identical value of $\Delta\phi\approx-0.7$ eV, we assume this is a reasonable assumption to describe interface effects at Co-TPP/noble-metal junctions. The

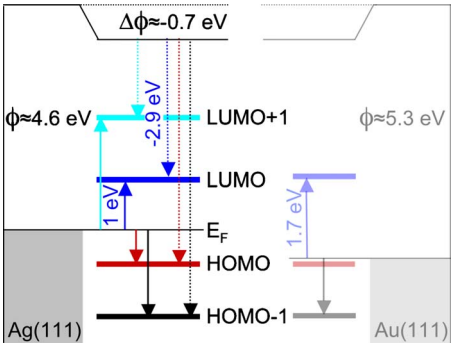

FIG. 8. (Color online) Diagram illustrating the energy-level alignment discussed in the text. The left part represents one monolayer of Co-TPP on Ag(111). The right part provides a tentative comparison with Co-TPP/Au(111), Ref. 42, assuming an identical work-function change.

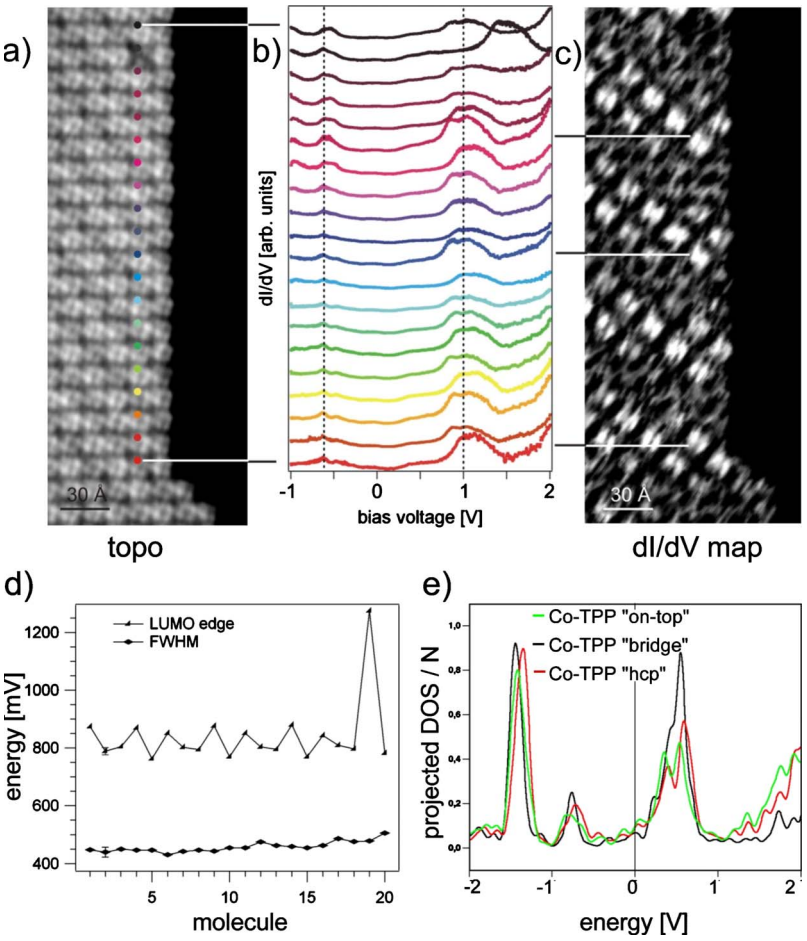

FIG. 9. (Color online) Spatial variation in the LUMO for Co-TPP/Ag(111). (a) Topographic STM image of the edge of a Co-TPP array. The colored dots mark the positions where the spectra represented in (b) were taken. (b) Series of STS spectra taken on the *meso*-carbon position for 20 Co-TPP molecules. The LUMO feature exhibits a spatial variation, that is clearly visualized as a superstructure, or Moiré-like pattern, in the dI/dV map of the LUMO displayed in (c) [(a) and (c): $V_b=1.1$ V and $I=0.17$ nA]. The second molecule from the top of the line is defective. (d) Variation in the LUMO onset energy and nearly constant FWHM of the LUMO. (e) Calculated density of state projected on the nitrogen p_z orbital for three different positions of the Co-TPP on Ag(111). The variation in the LUMO signature is reproduced by these calculations (see text for discussion).

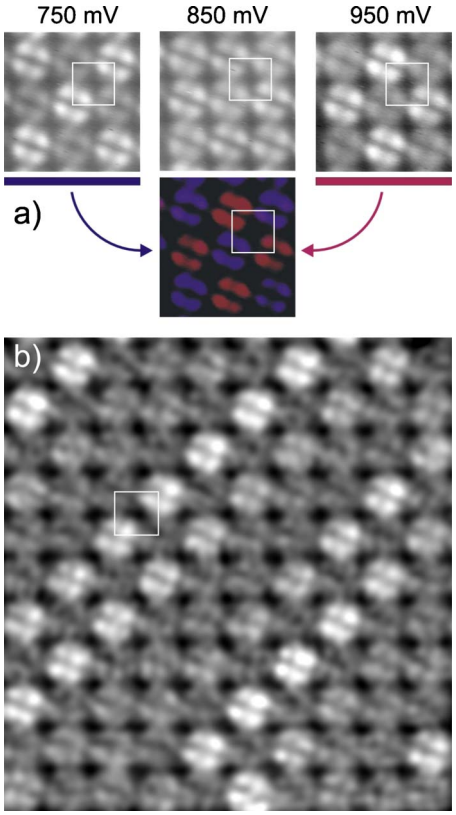

FIG. 10. (Color online) (a) Local view on a specific part of the LUMO superstructure by dI/dV maps [compare Fig. 9(c)]. In some regions of the superstructure a clear checkerboard-type intensity variation is observed, where the two molecules on one diagonal of the unit cell are bright, while the two others appear dim (I =0.6 nA). Due to the shifted LUMO onset and the varying intensity, this contrast inverts in a relatively small-energy window corresponding to 200 mV. This checkerboard structure is related to the noncommensurate structure of the Co-TPP arrays (compare Fig. 1 and see text for further discussion). The white square marks the unit cell of the Co-TPP overlayer. (b) dI/dV map on a larger area: the LUMO modulation does not constitute a regular checkerboard structure (I=0.3 nA and V_b=1 V, low-pass filtered).

resulting binding energies relative to the VL amount to −5.7 eV, −4.6 eV, and −2.8 eV. These values are strikingly close to our energies for the HOMO−1, HOMO, and LUMO, which indicates that the energy-level alignment follows the VL, thus indicating rather weak Co-TPP/substrate interactions for both Ag(111) and Au(111) surfaces. In addition, the binding energies of the HOMO−1 and the LUMO are reasonably close to the IP (−5.2 eV) and EA (−2.9 eV) reported for H_2-TPP molecules,[76] confirming that these states are mainly porphyrin macrocycle orbitals including only minor contributions from the metal center. The observation of nearly identical peak positions for HOMO−1 and LUMO in Co-TPP and Ni-TPP on Au(111) reported in Ref. 42 supports this interpretation.

Up to now, we only focused on intramolecular variations in the electronic structure of Co-TPP/Ag(111). Now we address the dependence of the electronic structure of a molecule on the location within an island. Figure 9 summarizes the observation of a spatial modulation of the LUMO within a densely packed layer. Taking spectra at identical positions (*meso*-carbon), but on different molecules, the tunneling spectra exhibit pronounced differences in the LUMO signature. The onset energy, as well as the relative intensity varies considerably from molecule to molecule while the overall full width at half maximum (FWHM) of the peak stays roughly constant [cf. Fig. 9(d)]. The resulting superstructure is most clearly visualized in dI/dV maps [cf. Fig. 9(c)] and shows similarity to a Moiré pattern. It should be noted that this effect is strongest for the LUMO orbital, very weak for the HOMO and absent for the LUMO+1 orbital on the phenyl legs.

Figure 10(a) shows a detailed view on the LUMO structure by comparing dI/dV maps taken at three different energies across the LUMO peak. We see that the contrast inverts within an energy range of only 200 meV. This effect is readily explained by the shifted onset energy in combination with the intensity variation in the LUMO. More interestingly, on this local scale, we observe a checkerboard structure with "bright" and "dim" molecules, i.e., the two molecules on one diagonal of the square unit cell appear bright, whereas the other two are dim. This contrast variation agrees nicely with the different registry of the molecules in the unit cell with the Ag(111) lattice [compare Fig. 1(c)]. Accordingly we suggest that the LUMO variations directly reflect the varying coupling of the Co-TPP to the Ag(111) surface. As the FWHM of the LUMO is roughly constant, we exclude a changing splitting of nearly degenerate states within the broad LUMO peak as origin for the superstructure. Such a hybridization effect would demand considerable molecule-substrate interactions, which is not consistent with our findings. We rather suggest that slight modifications of the Co-TPP-Ag bond length or subtle variations in the molecular conformation change the interface electronic structure. Indeed, the calculated density of states projected onto the p_z orbital of the N atoms of the macrocycle [cf. Fig. 7(e)], evaluated for Co-TPP molecules relaxed starting from on-top, hcp, and bridge adsorption sites, reveals a shift of the LUMO orbital as a function of the adsorption site. The energy of the feature related to the HOMO on the other hand is nearly identical for the three positions. The calculated structures reveal slight variations in the molecular geometry for the three positions ($\Delta\rho_{\mathrm{macro}}$: $\pm 4°$ and $\Delta\theta_{\mathrm{phenyl}}$: $\pm 8°$), going in hand with a variation in the vertical distance of the Co center to the outermost Ag layer from 2.8 to 2.9 Å. These values are in reasonable agreement with the 2.5 Å deduced from the PED analysis presented in Sec. III B.

An alternative explanation of the superstructure based on intermolecular interactions[77] or screening[78] seems unlikely, as the molecule-molecule distances are constant within the precision of our analysis and the LUMO is located on the macrocycle and not on the terminal groups, which might be more sensitive to intermolecular interactions. If the Co-TPP arrays constituted a perfect coincidence lattice with only two different adsorption sites, we would expect the superstructure to be a perfect checkerboard lattice of "bright" and "dim" molecules on a large scale. However, the checkerboard structure is only well developed on a very local scale, as it can be clearly seen in Figs. 9(c) and 10(b). In-between stripes exhibiting the checkerboard order, there are extended regions

without pronounced contrast variations, i.e., where no "bright" molecules are observed. This observation supports our statement of the Co-TPP arrays being noncommensurate with the Ag(111) atomic lattice. In contrast to the typical ordering principles for organic overlayers on metal substrates,[59] no low-index coincidence structure can describe the Moiré-type pattern observed for Co-TPP/Ag(111). This peculiar behavior of the Co-TPP is presumably related to the flexibility of the employed porphyrin unit. While we do not intend to speculate on an assignment of a given molecular contrast to a specific adsorption site on the Ag(111) substrate, it is reasonable to assume that the regions of less pronounced contrast within the superstructure [cf. Fig. 10(b)] are related to the quasi-hcp and quasi-fcc adsorptions sites, which give the strongest contribution to the PED pattern (compare Sec. III B).

IV. CONCLUSIONS

In summary, we presented a multimethod characterization of an archetypical porphyrin-noble-metal interface in exquisite detail. The combined approach allows us to capture comprehensively interrelated aspects that determine the geometric and electronic structure of the monolayer phase. The intermolecular Co-TPP interactions prevent the Co-TPP in densely packed molecular arrays from locking into unique adsorption sites of the underlying Ag(111) lattice. Accordingly, local STM observations reveal a Moiré-type contrast in the Co-TPP layers and space-averaging photoelectron diffraction patterns can only be modeled by including quasi-fcc and quasi-hcp adsorption sites. The resulting superstructure is directly reflected in variations in the LUMO of Co-TPP as evidenced by STS data. This site-specific modification of the LDOS assigned to the LUMO is supported by DFT calculations.

Furthermore the conformational adaptation of Co-TPP upon adsorption on Ag(111) was quantified by NEXAFS measurements. We find a saddle-shape deformation of the porphyrin macrocycle that is reflected in a twofold symmetric appearance of the Co-TPP in high-resolution STM images and apparent in the corresponding molecular orbitals as visualized by STS mapping. Both PED and DFT agree on a distance between Co centers and underlying substrate in the 2.5–3 Å range, consistent with the molecular deformation.

This knowledge of the geometric and electronic structure of the Co-TPP/Ag(111) interface is a prerequisite to rationalize the functionality of Co-TPP or related metalloporphyrin arrays on both simple and complex interfaces.[79,80] In addition, the information gained will be helpful to assess geometric shape and electronic properties of metalloporphyrin moieties in more intricate island or layer structures, respectively, in nanostructures or supramolecular architectures based on metalloporphyrin derivates with reactive *meso*-substituents.[81–87] More general, our experiments characterize a model system of an adsorbed flexible molecule and thus help to understand and predict the behavior of related species on other surfaces.

ACKNOWLEDGMENTS

Work supported by Canada Foundation of Innovation (CFI), National Science and Engineering research Council of Canada (NSERC), British Columbia Knowledge Development Fund (BCKDF), the ESF project FunSmarts, and the Munich Center for Advanced Photonics (MAP). W.A., A.W.-B., and J. R. thank the Swiss National Science Foundation (SNF), the German Academic Exchange Service (DAAD), and the Deutsche Forschungsgesellschaft (DFG), respectively. Traveling cost for the BESSY measurements provided by the BMBF through Grant No 05ES3XBA/5 is gratefully acknowledged. The authors thank Giorgio Zoppellaro and Mario Ruben (INT Karlsruhe) for providing high-purity Co-TPP molecules.

*wilhelm.auwaerter@ph.tum.de

[1] J. V. Barth, Annu. Rev. Phys. Chem. **58**, 375 (2007).
[2] F. Rosei, M. Schunack, Y. Naitoh, P. Jiang, A. Gourdon, E. Laegsgaard, I. Stensgaard, C. Joachim, and F. Besenbacher, Prog. Surf. Sci. **71**, 95 (2003).
[3] M. Castonguay, J.-R. Roy, A. Rochefort, and P. H. McBreen, J. Am. Chem. Soc. **122**, 518 (2000).
[4] S. M. Barlow and R. Raval, Surf. Sci. Rep. **50**, 201 (2003).
[5] H. Wende, M. Bernien, J. Luo, C. Sorg, N. Ponpandian, J. Kurde, J. Miguel, M. Piantek, X. Xu, P. Eckhold, W. Kuch, K. Baberschke, P. M. Panchmatia, B. Sanyal, P. M. Oppeneer, and O. Eriksson, Nature Mater. **6**, 516 (2007).
[6] C. Joachim, J. K. Gimzewski, and A. Aviram, Nature (London) **408**, 541 (2000).
[7] F. Chen, J. Hihath, Z. Huang, X. Li, and N. J. Tao, Annu. Rev. Phys. Chem. **58**, 535 (2007).
[8] S. R. Forrest, Chem. Rev. **97**, 1793 (1997).
[9] N. Koch, ChemPhysChem **8**, 1438 (2007).
[10] H. Ishii, K. Sugiyama, E. Ito, and K. Seki, Adv. Mater. **11**, 605 (1999).
[11] G. V. Nazin, X. H. Qiu, and W. Ho, Science **302**, 77 (2003).
[12] F. Moresco, L. Gross, M. Alemani, K.-H. Rieder, H. Tang, A. Gourdon, and C. Joachim, Phys. Rev. Lett. **91**, 036601 (2003).
[13] L. Grill, K.-H. Rieder, F. Moresco, S. Stojkovic, A. Gourdon, and C. Joachim, Nano Lett. **5**, 859 (2005).
[14] *The Porphyrins*, edited by D. Dolphin (Academic, New York, 1978).
[15] L. R. Milgrom, *The Colours of Life: An Introduction to the Chemistry of Porphyrins and Related Compounds* (Oxford University Press, New York, 1997).
[16] *The Porphyrin Handbook, Applications: Past, Present and Future*, edited by K. M. Kadish, K. M. Schmith, and R. Guilard (Academic Press, San Diego, 2000), Vol. 6.
[17] J. A. A. W. Elemans, R. van Hameren, R. J. M. Nolte, and A. E. Rowan, Adv. Mater. **18**, 1251 (2006).
[18] B. Hulsken, R. Van Hameren, J. W. Gerritsen, T. Khoury, P.

Thordarson, M. J. Crossley, A. E. Rowan, R. J. M. Nolte, J. A. A. W. Elemans, and S. Speller, Nat. Nanotechnol. **2**, 285 (2007).
[19] M. Gottfried and H. Marbach, Z. Phys. Chem. **223**, 53 (2009).
[20] N. Lin, S. Stepanov, M. Ruben, and J. V. Barth, Top. Curr. Chem. **287**, 1 (2009).
[21] J. V. Barth, Surf. Sci. **603**, 1533 (2009).
[22] L. Pan, S. Kelly, X. Huang, and J. Li, Chem. Commun. (Cambridge) **2002**, 2334.
[23] J. A. Shelnutt, X.-Z. Song, J. G. Ma, S.-L. Jia, W. Jentzen, and C. J. Medforth, Chem. Soc. Rev. **27**, 31 (1998).
[24] H. M. Marques and K. L. Brown, Coord. Chem. Rev. **225**, 123 (2002).
[25] E. B. Fleischer, C. K. Miller, and L. E. Webb, J. Am. Chem. Soc. **86**, 2342 (1964).
[26] S. J. Silvers and A. Tulinsky, J. Am. Chem. Soc. **89**, 3331 (1967).
[27] T. A. Jung, R. R. Schlittler, and J. K. Gimzewski, Nature (London) **386**, 696 (1997).
[28] F. Moresco, G. Meyer, K.-H. Rieder, J. Ping, H. Tang, and C. Joachim, Surf. Sci. **499**, 94 (2002).
[29] W. Auwärter, A. Weber-Bargioni, A. Riemann, A. Schiffrin, O. Gröning, R. Fasel, and J. V. Barth, J. Chem. Phys. **124**, 194708 (2006).
[30] T. Yokoyama, S. Yokoyama, T. Kamikado, and S. Mashiko, J. Chem. Phys. **115**, 3814 (2001).
[31] X. H. Qiu, G. V. Nazin, and W. Ho, Phys. Rev. Lett. **93**, 196806 (2004).
[32] V. Iancu, A. Deshpande, and S.-W. Hla, Nano Lett. **6**, 820 (2006).
[33] W. Auwärter, A. Weber-Bargioni, S. Brink, A. Riemann, A. Schiffrin, M. Ruben, and J. V. Barth, ChemPhysChem **8**, 250 (2007).
[34] K. Ogaki, N. Batina, M. Kunitake, and K. Itaya, J. Phys. Chem. **100**, 7185 (1996).
[35] M. Kunitake, U. Akiba, N. Batina, and K. Itaya, Langmuir **13**, 1607 (1997).
[36] T. Shimada, R. Hashimoto, J. Koide, Y. Kamimuta, and A. Koma, Surf. Sci. **470**, L52 (2000).
[37] Y. He, T. Ye, and E. Borguet, J. Am. Chem. Soc. **124**, 11964 (2002).
[38] K. Suto, S. Yoshimoto, and K. Itaya, Langmuir **22**, 10766 (2006).
[39] H. Suzuki, S. Berner, M. Brunner, H. Yanagi, D. Schlettwein, T. A. Jung, and H.-J. Güntherodt, Thin Solid Films **393**, 325 (2001).
[40] L. Scudiero, D. E. Barlow, and K. W. Hipps, J. Phys. Chem. B **104**, 11899 (2000).
[41] L. Scudiero, K. W. Hipps, and D. E. Barlow, J. Phys. Chem. B **107**, 2903 (2003).
[42] L. Scudiero, D. E. Barlow, U. Mazur, and K. W. Hipps, J. Am. Chem. Soc. **123**, 4073 (2001).
[43] A. Weber-Bargioni, W. Auwärter, F. Klappenberger, J. Reichert, S. Lefrancois, T. Strunskus, C. Wöll, A. Schiffrin, Y. Pennec, and J. V. Barth, ChemPhysChem **9**, 89 (2008).
[44] VTS-CreaTec GMBH, D-74391 Erligheim, Germany.
[45] G. Meyer, Rev. Sci. Instrum. **67**, 2960 (1996).
[46] G. Zoppellaro and M. Ruben, INT Karlsruhe, D-76021 Karlsruhe, Germany.
[47] L. Floreano, G. Naletto, and D. Cvetko, Rev. Sci. Instrum. **70**, 3855 (1999).
[48] T. Lukasczyk, K. Flechtner, L. R. Merte, N. Jux, F. Maier, J. M. Gottfried, and H.-P. Steinrück, J. Phys. Chem. C **111**, 3090 (2007).
[49] M. Vladimirova, G. Trimarchi, A. Baldereschi, J. Weckesser, K. Kern, J. V. Barth, and A. De Vita, Acta Mater. **52**, 1589 (2004).
[50] M. Rohlfing, R. Temirov, and F. S. Tautz, Phys. Rev. B **76**, 115421 (2007).
[51] F. Klappenberger, M. E. Cañas-Ventura, S. Clair, S. Pons, U. Schlickum, Z.-R. Qu, H. Brune, K. Kern, T. Strunskus, C. Wöll, A. Comisso, A. De Vita, M. Ruben, and J. V. Barth, ChemPhys Chem **8**, 1782 (2007).
[52] G. Kresse and J. Furthmüller, Comput. Mater. Sci. **6**, 15 (1996).
[53] P. E. Blöchl, Phys. Rev. B **50**, 17953 (1994).
[54] G. Kresse and D. Joubert, Phys. Rev. B **59**, 1758 (1999).
[55] K. Comanici, F. B. K. Flechtner, T. Lukasczyk, J. M. Gottfried, H. P. Steinrück, and H. Marbach, Langmuir **24**, 1897 (2008).
[56] J. Brede, M. Linares, S. Kuck, J. Schwöbel, A. Scarfato, S.-H. Chang, G. Hoffmann, R. Wiesendanger, R. Lensen, P. H. Kouwer, J. Hoogboom, A. E. Rowan, M. Bröring, M. Funk, S. Stafström, F. Zerbetto, and R. Lazzaroni, Nanotechnology **20**, 275602 (2009).
[57] S. Tsuzuki, K. Honda, T. Uchimaru, M. Mikami, and K. Tanabe, J. Am. Chem. Soc. **124**, 104 (2002).
[58] O. Bludský, M. Rubeš, P. Soldán, and P. Nachtigall, J. Chem. Phys. **128**, 114102 (2008).
[59] D. E. Hooks, T. Fritz, and M. D. Ward, Adv. Mater. **13**, 227 (2001).
[60] http://electron.lbl.gov/mscdpack/mscdpack.html, also see Ref. 61.
[61] Y. Chen, F. J. García de Abajo, A. Chassé, R. X. Ynzunza, A. P. Kaduwela, M. A. Van Hove, and C. S. Fadley, Phys. Rev. B **58**, 13121 (1998).
[62] J. Stöhr, *NEXAFS Spectroscopy and the Structure of Molecules Bonded to Surfaces* (Springer, New York, 1991).
[63] W. Auwärter, F. Klappenberger, A. Weber-Bargioni, A. Schiffrin, T. Strunskus, C. Wöll, Y. Pennec, A. Riemann, and J. V. Barth, J. Am. Chem. Soc. **129**, 11279 (2007).
[64] F. Klappenberger, A. Weber-Bargioni, W. Auwärter, M. Marschall, A. Schiffrin, and J. V. Barth, J. Chem. Phys. **129**, 214702 (2008).
[65] K. Weiss, S. Gebert, M. Wühn, H. Wadepohl, and C. Wöll, J. Vac. Sci. Technol. A **16**, 1017 (1998).
[66] D. Duflot, J.-P. Flament, J. Heinesch, and M.-J. Hubin-Franskin, J. Electron Spectrosc. Relat. Phenom. **113**, 79 (2000).
[67] C. C. Cudia, P. Vilmercati, R. Larciprete, C. Cepek, G. Zampiere, L. Sangaletti, S. Pagliara, A. Verdini, A. Cossaro, L. Floreano, A. Morgante, L. Petaccia, S. Lizzit, C. Battocchio, G. Polzonietti, and A. Goldoni, Surf. Sci. **600**, 4013 (2006).
[68] S. Müllegger, W. Schöfberger, M. Rashidi, M. L. Reith, and R. Koch, J. Am. Chem. Soc. **131**, 17740 (2009).
[69] A. Rosa, G. Ricciardi, and E. J. Baerends, J. Phys. Chem. A **110**, 5180 (2006).
[70] M. Ziegler, N. Néel, A. Sperl, J. Kröger, and R. Berndt, Phys. Rev. B **80**, 125402 (2009).
[71] A. Weber-Bargioni, J. Reichert, A. P. Seitsonen, W. Auwärter, A. Schiffrin, and J. V. Barth, J. Phys. Chem. C **112**, 3453 (2008).
[72] L. A. Zotti, G. Teobaldi, W. A. Hofer, W. Auwärter, A. Weber-Bargioni, and J. V. Barth Surf. Sci. **601**, 2409 (2007).
[73] F. Buchner, K.-G. Warnick, T. Wölfle, A. Görling, H.-P. Steinrück, W. Hieringer, and H. Marbach, J. Phys. Chem. C **113**,

16450 (2009).
[74] A. Alkauskas, L. Ramoino, S. Schintke, M. von Arx, A. Baratoff, H.-J. Güntherodt, and T. A. Jung, J. Phys. Chem. B **109**, 23558 (2005).
[75] W. Auwärter, F. Klappenberger, K. Seufert, A. Weber-Bargioni, and J. V. Barth (unpublished).
[76] M. Tao, X. Zhou, M. Jing, D. Liu, and J. Xing, Dyes Pigm. **75**, 408 (2007).
[77] L. Gross, K.-H. Rieder, A. Gourdon, C. Joachim, and F. Moresco, ChemPhysChem **8**, 245 (2007).
[78] I. F. Torrente, K. J. Franke, and J. I. Pascual, J. Phys.: Condens. Matter **20**, 184001 (2008).
[79] V. Iancu, A. Deshpande, and S.-W. Hla, Phys. Rev. Lett. **97**, 266603 (2006).
[80] M. Bernien, J. Miguel, C. Weis, M. E. Ali, J. Kurde, B. Krumme, P. M. Panchmatia, B. Sanyal, M. Piantek, P. Srivastava, K. Baberschke, P. M. Oppeneer, O. Eriksson, W. Kuch, and H. Wende, Phys. Rev. Lett. **102**, 047202 (2009).
[81] L. Grill, M. Dyer, L. Lafferentz, M. Persson, M. V. Peters, and S. Hecht, Nat. Nanotechnol. **2**, 687 (2007).
[82] M. I. Veld, P. Iavicoli, S. Haq, D. B. Amabilino, and R. Raval, Chem. Commun. (Cambridge) **2008**, 1536.
[83] H. Spillmann, A. Kiebele, T. A. Jung, D. Bonifazi, F. Cheng, and F. Diederich, Adv. Mater. **18**, 275 (2006).
[84] F. Buchner, K. Seufert, W. Auwärter, D. Heim, J. V. Barth, K. Flechtner, J. M. Gottfried, H.-P. Steinrück, and H. Marbach, ACS Nano **3**, 1789 (2009).
[85] L.-A. Fendt, M. Stöhr, N. Wintjes, M. Enache, T. A. Jung, and F. Diederich, Chem.-Eur. J. **15**, 11139 (2009).
[86] D. Heim, K. Seufert, W. Auwärter, C. Aurisicchio, C. Fabbro, D. Bonifazi, and J. V. Barth, Nano Lett. **10**, 122 (2010).
[87] D. Heim, D. Écija, K. Seufert, W. Auwärter, C. Aurisicchio, C. Fabbro, D. Bonifazi, and J. V. Barth, J. Am. Chem. Soc. **132**, 6783 (2010).